CONTENTS

CHAPTER 1

TYCHO'S SIX: HIGH-RESOLUTION SPECTROSCOPY SEARCH FOR THE REMAINING DONOR FOR THE TYCHO SUPERNOVA

1.1. Introduction

Type Ia Supernovae (SNe Ia) are of great interest for astronomy. They represent some of the most extreme physical situations in stellar astronomy, produce substantive amounts of Iron group elements which impacts the chemical evolution of galaxies and the Universe, and are uniquely powerful probes of Cosmic distance. applications in stellar and galactic astronomy as well as in cosmology. Despite their wide ranging significance, fundamental uncertainties remain around progenitor of these cataclysmic events.

There is general consensus that SNe Ia are caused by the deflagration/detonation of a Carbon/Oxygen white dwarf which is accreting material from a binary companion. Scenarios exists where the explosion can be initiated from a detonation on the surface of the star (reference of Livne, and Sim), through runaway carbon burning in the white dwarfs interior, or through a cataclysmic merger of objects.

Observationally, two main scenarios for this accretion process can be identified.. The first scenario sees the accretion process occurring through Roche Lobe Overflow (henceforth RLOF) of a close non-degenerate companion (also known as donor star). This companion, which has undergone common envelope evolution with the white dwarf, can be a helium, main-sequence, sub-giant, or red giant star. is a main-sequence to red giant star at the time of the explosion (SD scenario). In all cases the donor star should survive the explosion and remains visible post-explosion.

The second scenario is the dynamical merger of two white dwarfs (DD scenario). In this scenario, the co-evolution of two stars eventually leads to a close binary of two white dwarfs, which are able, through the emission of gravitational radiation, to merge over a wide range of times after the initial formation of the system. In most cases this would leave no remaining star (e.g. Pakmor et al., 2010).

Both scenarios have support in observation and theory. The detection of circum-stellar material around certain SN Ia, such as SN 2006X (Patat et al., 2007), provides support for the SD model. On the other hand the lack of substantial hydrogen in in the majority of other SNe Ia (Leonard, 2007) poses a challenge to the SD scenario.

Kasen (2010) suggests that the interaction with the non-degenerate companion should imprint an observable signature on a SN Ia light curve, depending on viewing angle, and radius of the companion. Such an excess has not yet been observed (Hayden et al., 2010; Tucker, 2011; Bianco et al., 2011).which is at odds with Red Giant companions forming the majority of SNe Ia.

Population synthesis calculations are challenging, with various authors getting different results for the same inputs (Nelemans paper). However there is a general trend from these calculations that neither single-degenerate nor double degenerate stars can provide enough systems to explain the SN Ia rate (Ruiter et al., 2009; Mennekens et al., 2010; **?**; Han, 2008). Several authors suggest the population might comprise both single and double degenerate systems.

The physics of white dwarf mergers is challenging to numerically simulate, but in the simplest calculations, these mergers will lead to the formation of a neutron star (Saio & Nomoto, 1985). Recently Pakmor et al. (2010) have shown that for certain parameters (white dwarf binaries with a mass ratio very close to one) the merger may explain sub-luminous supernovae.

To investigate the nature of progenitors observationally Ruiz-Lapuente et al. (2004, henceforth RP04) have tried to directly detect donor stars in SN Ia remnants within the Milky Way. They have identified two historical Galactic SN well suited to this task - SN 1006 and Tycho's SN (SNR1572 henceforth). Both remnants are young (440 and 1000 years old, respectively), almost certainly SN Ia from both their observational signatures (RP 04 but not RP04), Badenes et al. (look it up), and not overwhelmed by Galactic extinciton. In this paper, we will focus on SN1572.

SNR1572 is relatively close (2.8 ± 0.8 kpc), very young and has been confirmed as a normal SN Ia remnant (Badenes et al., 2006; Krause et al., 2008). While the star has an unusual spatial motion compared to other stars in the field, its current location and proper motion place it a significant distance from the remnants center - a feature difficult to explain in connecting Tycho-G to SNR1572.

RP04 investigated most bright stars in the central regions of SN1572 and found a star with an unusual spatial motion (Tycho-G by their nomenclature) and suggested this as a possible donor star for SN1572. One consequence of RLOF is a rotational velocity induced on the donor star by tidal locking in the system. This results in an unusually large rotationally velocity, related to the orbital velocity of the binary system and can be used to single out donor stars against nearby unrelated stars. (Kerzendorf et al., 2009, ,henceforth WEK09) investigated rotation for Tycho-G but found no excess rotation velocity compared to a normal star. WEK09's measurements of Tycho-G, including a revised radial velocity, compared to a Galactic models, showed it is statistically consistent with an interloping star. However, WEK09 were able to provide an a priori unlikely scenario, where the star was able to lose its rotational signature.

Hernandez et al. (2009, henceforth GH09) analysed a spectrum of Tycho-G observed with the HIRES-instrument on the Keck telescope. GH09confirmed WEK09's radial velocity for Tycho-G and determined its stellar parameters and metallicities. GH09in addition to

refining the metallicity, Temperature and Gravity measurements for Tycho-G, concluded concluded that Tycho-G has an unusually large amount of Ni. GH09 claim that this Ni measurement could be attributed to the accretion of ejecta material on the donor star.

In this paper we analyse HIRES spectra of the 6 bright stars in SNR1572 center. These spectra were taken by the same program that obtained the data used by GH-09, and we independently reanalyze this spectrum as part of our program.

We describe the observational data and our data reduction procedures in Section 1.2. Section 1.3 is divided into five subsections detailing the measurements of proper motion, radial velocity, rotation, stellar parameters and abundances. In Section 1.4 we analyse the measurements of each star to investigate its potential association with SNR1572, and present our conclusion in section 1.5.

1.2. Observations and Data Reduction

We obtained spectra with the High Resolution Echelle Spectrograph (HIRES Vogt et al., 1994) on the Keck 10m telescope in Mauna Kea. The observations were made on two nights on 2006 September 10 and 2006 October 11. The slits B5 and C1 (with the same width of 0.86'' but different lengths, B5 length 3.5'', C1 length 7.0'') were used resulting in a wavelength coverage of 3930 – 5330 Å, 5380 – 6920 Å and 6980 – 8560 Å with $R \approx 50,000$, providing us with the necessary spectral resolution and wavelength coverage to determine stellar parameters. The spectra were reduced using the MAKEE package. All spectra were corrected to heliocentric velocities, using the MAKEE skyline method. The spectra were not corrected for telluric lines as they will not influence our analysis of the stellar parameters. The final exposure times of the combined spectra for each candidate and signal to noise ratio at 4000-4100 Å are shown in Table 1.1. Finally we normalized the spectrum using the IRAF-Task continuum. We note that Tycho-C and Tycho-D were observed on the same slit (C1) with a separation of 2.1''.

In addition, we obtained low-resolution spectroscopy ($R \approx 1200$) of Tycho-B with the dual-arm Low-Resolution Imaging Spectrometer (LRIS; Oke et al., 1995) mounted on the 10-m Keck I telescope. The observations were taken on one run on 2010 November 07, using only the blue arm with the 600/4000 grism and the 1'' wide slit. This resulted in a wavelength coverage of 3200 – 5600 Å. These observations were taken to obtain a precise measurement of the surface gravity for Tycho-B using the size of the Balmer decrement. The spectrum of Tycho-B was reduced using standard techniques (e.g. Foley et al., 2003).

Table 1.1 Observations of Stars

Name designation	RA (J2000) (hh:mm:ss.ss)	Dec (J2000) (dd:mm:ss.ss)	Date (dd/mm/yy)	Slit	t_{exp} (s)	S/N
Tycho-A	00:25:19.73	+64:08:19.6	10/09/06	B5	900	≈ 65
Tycho-B	00:25:19.95	+64:08:17.11	10/09/06	B5	1200	≈ 50
Tycho-C	00:25:20.40	+64:08:12.32	11/10/06	C1	10800	≈ 10
Tycho-D	00:25:20.60	+64:08:10.82	11/10/06	C1	10800	≈ 5
Tycho-E	00:25:18.29	+64:08:16.12	11/10/06	C1	9000	≈ 15
Tycho-G	00:25:23.58	+64:08:02.06	10/09/06 & 11/10/06	B5&C1	24000	≈ 30

Routine CCD processing and spectrum extraction were completed with IRAF[1], and the data were extracted with the optimal algorithm of Horne (1986). We obtained the wavelength scale from low-order polynomial fits to calibration-lamp spectra. Small wavelength shifts were then applied to the data after measuring the offset by cross-correlating a template sky to the night-sky lines that were extracted with the star. Using our own IDL routines, we fit a spectrophotometric standard-star spectrum to the data in order to flux calibrate Tycho-B and remove telluric lines (Horne, 1986; Matheson et al., 2000).

1.3. Analysis

1.3.1. Astrometry

Proper motions can be used to identify potential donor stars because donor stars freely travel with their orbital velocity after the SN explosion disrupts the system. RP04 suggested Tycho-G as a possible donor due to its unusually high proper motion and unusually high radial velocity. For this work we measured proper motions for 201 stars within one arcminute of the remnant's center. We used archival HST images for three different epochs (HST Program ID 9729 & 10098; November 2003, August 2004, May 2005) each consisting of three exposures (1 s, 30 s and 1440 s) in the F555W using the Advance Camera for Surveys (ACS). The pixel size in each exposure is 50 mas pixel^{-1}. This dataset results in a maximum baseline of 30 months.

We used an image from the middle epoch (2004) to establish a reference frame and oriented the pixel coordinate system with the equatorial system. We then applied a distortion correction for the F555W filter (Anderson & King, 2006) to each images and then calculated transformations (order xxxxx) between all other images and the reference image. We then used these transformations to calculate the position of all stars in the reference coordinate system with the overall uncertainty of each position estimated (How?). Some faint stars where not detected in the shorter exposures and were thus excluded from proper motion measurements (with 114 Stars remaining).

For each star, we fit a linear regression for the stellar positions over time in the pixel coordinates (which were aligned with the equatorial system). The x and y data were treated as independent measurements, with separate regressions solved for each axis directions. Errors were estimate using standard least squares analysis and the individual error estimates each object's positions.

There are three measurements of the geometric center of SN1572 using different datasets. Reynoso et al. (1997) using VLA data determined the center to R.A. 00:25:14.95 Dec +64:08:05.7 J2000, Hughes (2000) using ROSAT data got R.A. 00:25:19 Dec +64:08:10 J2000 and Warren et al. (2005) with Chandra data determined the center to R.A. 00:25:19.40 Dec +64:08:13.98 J2000.

Table 1.2 lists the proper motions and errors of all stars mentioned in RP04 (19 stars) which were analyzed in this work as well as the distance to the geometric X-Ray center measured by Chandra.

[1]IRAF: the Image Reduction and Analysis Facility is distributed by the National Optical Astronomy Observatory, which is operated by the Association of Universities for Research in Astronomy (AURA) under cooperative agreement with the National Science Foundation (NSF).

Table 1.2 Proper motion of Candidates

Name designation	RA (J2000) (hh:mm:ss.ss)	Dec (J2000) (dd:mm:ss.s)	μ_α mas yr^{-1}	μ_δ mas yr^{-1}	$\Delta\mu_\alpha$ mas yr^{-1}	$\Delta\mu_\delta$ mas yr^{-1}''	r
B	0:25:19.97	64:08:17.1	-1.24	0.56	0.62	0.64	4.86
A	0:25:19.73	64:08:19.8	-0.09	-0.89	1.17	0.90	6.21
A2	0:25:19.81	64:08:20.0	-0.71	-3.60	0.69	0.64	6.58
C	0:25:20.38	64:08:12.2	-0.21	-2.52	0.65	0.65	6.66
E	0:25:18.28	64:08:16.1	2.04	0.54	0.66	0.69	7.60
D	0:25:20.62	64:08:10.8	-1.12	-1.99	1.01	0.86	8.60
1	0:25:16.66	64:08:12.5	-2.27	-1.37	1.60	1.15	18.00
F	0:25:17.09	64:08:30.9	-4.41	0.20	0.70	0.71	22.69
J	0:25:15.08	64:08:05.9	-2.40	-0.25	0.62	0.62	29.44
G	0:25:23.58	64:08:01.9	-2.50	-4.22	0.60	0.60	29.87
R	0:25:15.51	64:08:35.4	0.28	0.24	0.89	0.80	33.23
N	0:25:14.73	64:08:28.1	1.18	0.89	0.86	0.98	33.66
U	0:25:19.24	64:07:37.9	0.01	-3.04	0.73	0.75	36.06
Q	0:25:14.81	64:08:34.2	1.45	3.07	0.64	0.72	36.19
T	0:25:14.58	64:07:55.0	-3.85	0.52	0.72	0.62	36.78
K	0:25:23.89	64:08:39.3	0.18	0.17	0.73	0.69	38.73
L	0:25:24.30	64:08:40.5	0.16	-0.44	0.75	0.82	41.59
S	0:25:13.78	64:08:34.4	4.16	0.58	0.83	0.84	42.09
2	0:25:22.44	64:07:32.4	74.85	-4.43	0.82	0.83	46.09

We compared the distribution of proper motions of all measured stars to ours candidates in Figure 1.1.

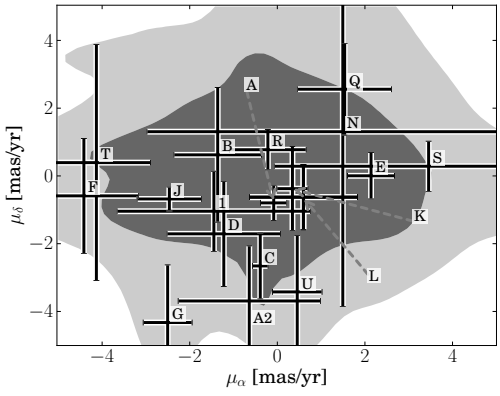

Figure 1.1 The contours show the distribution of proper motion ($1-\sigma$ and $2-\sigma$) excluding the named stars. We show the location of the candidate stars and their errors on top of this distribution. Tycho-2 was not shown in this figure as it is an extreme outlier with $\mu_\alpha = 75$ mas yr^{-1} and $\mu_\delta = -4.4$ mas yr^{-1} but also at a large distance to the center of the remnant's geometric center (46'').

Table 1.3 Radial velocities

Name designation	Date (dd/mm/yy)	$v_{\rm helio}$ (km s^{-1})	$v_{\rm LSR}$ (km s^{-1})	Δv (km s^{-1})
Tycho-A	09/09/06	-36.79	-28.5	0.23
Tycho-B	09/09/06	-55.0	-57.0	≈ 2
Tycho-C	11/10/06	-58.78	-50.49	0.75
Tycho-D	11/10/06	-58.93	-50.64	0.78
Tycho-E	11/10/06	-64.2	-55.91	0.27
Tycho-G	09/09/06	-87.12	-78.83	0.25
Tycho-G	11/10/06	-87.51	-79.22	0.78

1.3.2. Radial Velocity

The radial velocity of each star was measured using the IRAF task *fxcor* (Tonry & Davis, 1979). MAKEE was used to calculate an intrinsic velocity shift by comparing offsets of the nightsky-lines. The radial velocity standards were reduced in the same fashion.

Each order of each star was then cross-correlated with at least two other radial velocity standards (HR6349, HR6970, HR1283) which had been observed on the same night.

The radial velocity for Tycho-B was measured in the course of determining the stellar parameters for Tycho-B with the stellar parameter fitting package *sfit* (Jeffery et al., 2001). The *sfit* result consistently gives $v_{\rm helio} = -55$ km s^{-1} for different stellar parameters with an error of ≈ 2 km s^{-1}.

In Table 1.3 we have listed all the radial velocities both in a heliocentric frame and a local-standard-of-rest (henceforth LSR) frame. We will be referring to the heliocentric measurements from here on. The listed error is the standard deviation of the radial velocity measurement of all orders added in quadrature to the error of the radial velocity standards.

In Figure 1.2 we have compared the radial velocity of our sample stars to radial velocities of stars in the direction of Tycho's SNR using the Besançon Model (Robin et al., 2003). The distance as well as the error in distance are taken from Section 1.3.5. The candidates radial velocities are all typical for their distance. Finally, we note the measurement of Tycho-G is consistent with WEK09 and GH09.

1.3.3. Rotational Velocity

We have measured rotational velocities of all stars except Tycho-B in the same fashion as described in WEK09. We selected several unblended and strong (but not saturated) FeI lines in the stellar spectra . We added these lines after shifting them to the same wavelength and scaling them to the same equivalent width. This was done to improve the signal to noise ratio for the faint stars as well as providing consistency throughout all stars.

As a reference we created three synthetic spectra for each star (one broadened only with the instrumental profile, the others with the instrumental profile and $v_{\rm rot} \sin i$ of 10 and 13 km s^{-1} respectively) with the 2010 version of MOOG (Sneden, 1973), using our derived temperature, gravity and metallicity. As input data to MOOG we used the Castelli & Kurucz (2004) atmospheric models and a line list from Kurucz & Bell (1995). We then applied the same process of line selection and adding as for the lines in the observed

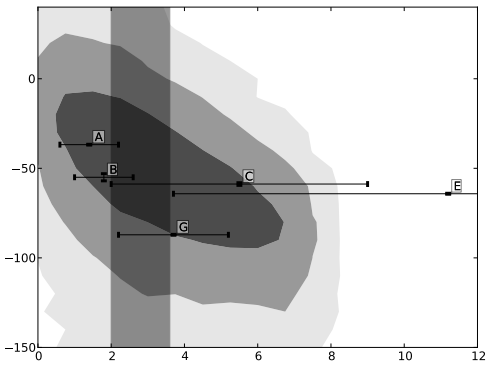

Figure 1.2 The contours indicate 1, 2 and 3 − σ levels of the distance and radial velocity using the Besançon Model (Robin et al., 2003) with ≈ 60000 stars in the direction of SNR1572 (only including star with a V between 10 and 20 as well as stars with a metallicity of [Fe/H] > −1). We have overplotted our candidate stars with error bars. One should note that the errors in distance are only an indication of the error, the proper error surfaces can be seen in Figure 1.6. The vertical gray shade shows the error range for the distance of SNR1572.

spectra.

Figure 1.3 shows the comparison between the synthetic spectra of different rotational velocity and the observed spectra. This comparison indicates that the stellar broadening (rotational, macro turbulence, etc.) is less than broadening due to the instrumental profile of 6 km s^{-1} for each star. We adopt 6 km s^{-1} as an upper limit to the rotation for all stars.

Due to its high temperature and rotation, we fit the rotational velocity for Tycho-B with the program *sfit* (Jeffery et al., 2001, described in section 1.3.4) as part of the overall fit for this star's stellar parameters. We find $v_{\rm rot} = 171^{+16}_{-33}$ km s^{-1}. While Tycho-B's rotation is very high compared to the other candidate stars, for stars of this temperature and gravity a high rotation is not unusual.

In summary, none of the stars show rotation which is measurable at this resolution.

1.3.4. Stellar parameters

The stellar parameters are presented in Table **??** and were determined using a traditional spectroscopic approach based on the equivalent widths of lines of different excitation and ionization levels. . These measurements exclude Tycho-B, due to its hot temperature, and we measure its stellar parameters by direct comparison to models, in a separate procedure.

Equivalent widths (EWs) for a set of Fe lines were measured using routines in IRAF (compiled from Reddy et al. (2003, henceforth Reddy03) and Ramírez & Cohen (2002, henceforth RC02) Table **??** shows the EWs measured for each of the stars. Missing values indicate that the line was not detected.

We used the local thermodynamic equilibrium (LTE) stellar line analysis program MOOG (Sneden, 1973) and LTE model atmospheres from the Castelli & Kurucz (2003) grid to derive an abundance for a given line. The effective temperature, $T_{\rm eff}$, was adjusted until the abundances from FeI lines displayed no trend as a function of excitation potential. The surface gravity, $\log g$, was adjusted until the abundances from FeI and FeII lines were in agreement. The microturbulent velocity, ξ_t , was adjusted until there was no trend between the abundances from the FeI lines and EW. This process was iterated until self

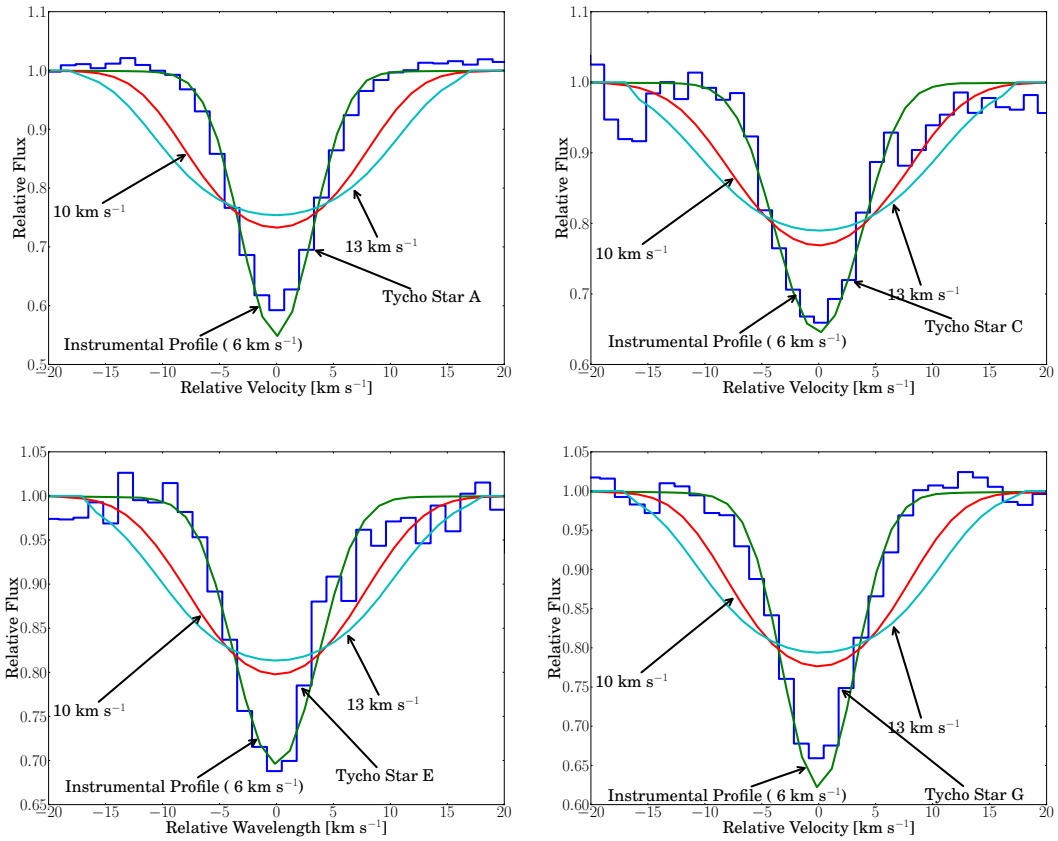

Figure 1.3 The figures show the combination of Fe-line profiles after normalization to the same equivalent width and compare them to synthetic line profiles created by MOOG. We convolved the synthetic lines first with a rotational kernel with three different values for rotation and then with the instrumental profile. All stars show rotation less than 6 km s^{-1} which is equal to the instrumental profile at this resolution.

consistent stellar parameters were obtained for each star. In our analysis, we explored stellar parameters at discrete values. For $T_{\rm eff}$, we considered values at every 25 K (e.g., 4000, 4025 K, etc.), for $\log g$, we considered values at every 0.05 dex (e.g., 1.00, 1.05 dex, etc.), and for ξ_t , we considered values at every 0.05 km s^{-1}(e.g., 1.70, 1.75 km s^{-1}, etc.). We assumed that excitation equilibrium was satisfied when the slope between $\log \epsilon$(FeI) and lower excitation potential (χ) was ≤ 0.004. We assumed that ionization equilibrium was achieved when $|\log \epsilon(\text{FeI}) - \log \epsilon(\text{FeII})| \leq 0.02$ dex. The microturbulent velocity was set when the slope between $\log \epsilon$(FeI) and reduced equivalent width ($\log \text{W}/\lambda$) was ≤ 0.004. In all cases we found appropriate solutions in which the trends between Fe I, Fe II, EW and excitation potentials were small. We estimate that the internal errors are typically $T_{\rm eff} \pm 100$ K, $\log g \pm 0.3$ dex, and $\xi_t \pm 0.3$ km s^{-1}. For further details regarding the derivation of stellar parameters, see Yong et al. (2008).

The final iron measurements are the average of FeI and FeII assuming the solar abundances of Asplund et al. (2009) In addition, we measured abundance for the Elements Ni and Li via EW analysis. We could not see any unusual abundance pattern for any of the sample stars (see Figure 1.4; Tycho-B's abundances are not presented on the plot as they were measured in a different fashion).

In summary, the inferred metallicities for all candidates show that the candidates are

Table 1.4 Stellar Parameters

Name designation	$T_{\rm eff}$ (K)	$\log g$ (dex)	[Fe/H] (dex)	Δ[Fe/H] (dex)	[Ni/H] (dex)	Δ[Ni/H] (dex)	[Li/H] (dex)
Tycho-A	4975	2.9	0.02	0.16	0.05	0.025	0.09
Tycho-C	4950	2.9	-0.57	0.23	-0.14	-0.17	0.11
Tycho-E	5825	3.4	-0.16	0.21	0.2	0.0	0.131
Tycho-G	6025	4	-0.15	0.18	0.14	0.08	0.11

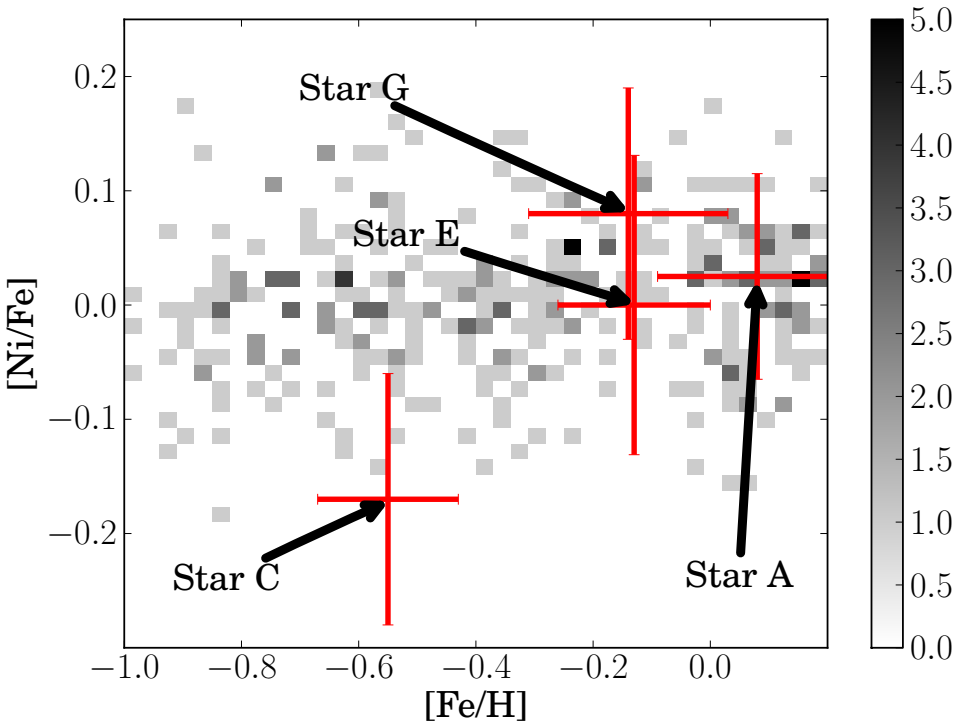

Figure 1.4 The background colour indicates the distribution is taken from Kobayashi et al. (2006). All of the measured candidates are consistent within the errors with stars of the same metallicity.

of roughly solar metallicities with the exception of the metal-poor Tycho-C. The range of metallicities spanned by the program stars is compatible with membership of the thin disk (REFERENCE). Based on metallicity alone, we do not regard any of the program stars to be unusually metal-poor or metal-rich. Additionally, we find the [Ni/Fe] abundance to be consistent with stars of similar metallicity (see Figure 1.4). The stellar paramaters and elemental abundances are listed in Table 1.4.

Because Tycho B has a temperature greater than 9000 K and is quickly rotating, the process described above cannot be used to measure stellar parameters. Instead we used the program *sfit* (Jeffery et al., 2001) to match the HIRES-spectrum to a grid of model spectra. To determine the stellar parameters for Tycho-B we have used a model grid with [Fe/H] = −1.0, 8000 < $T_{\rm eff}$ < 16000, 7 < $\log g$ < 2. This low metallicity is suggested by a very weak Calcium K line and Mg II lines, but is hard to measure. We can not measure Helium directly in this spectrum and thus adopt N(He) = 0.1 as this is empirically a very

Table 1.5 Tycho-B abundances

Ion designation	λ Å	W_λ Å	ϵ dex	$[X/H]$ dex	$\frac{\partial\epsilon}{\partial \log g}$	$\frac{\partial\epsilon}{\partial T_{\rm eff}}$ K^{-}1
MgII	4481.13+4481.33	220 ± 15	6.18 ± .08	-1.40	0.08	8×10^{-5}
SiII	6347.1	140 ± 5	6.96 ± .18	-0.59	-0.02	1×10^{-4}
OI	7771.9+7774.2+7775.4	460 ± 30	8.43 ± .10	-0.58	0.24	-4×10^{-5}

common Helium abundance in stars.

This analysis resulted in $T_{\rm eff} = 10000^{+400}_{-200}$ K, $\log g = 3.67$ with slope $\partial \log g/\partial T_{\rm eff} = 0.27/500\,{\rm K}^{-1}$, rotational velocity $v \sin i = 171$ km s^{-1} with slope $\partial v \sin i/\partial T_{\rm eff} = -41/500$ km s^{-1} K^{-1}. From qualitative analysis this object seems metal poor (e.g. in comparison to stars of similar stellar parameters but solar metallicity), but its high rotation and temperature make it hard to determine this parameter precisely. For the present, we assume [Fe/H] = -1.0 unless otherwise noted.

In addition, using the high-resolution spectrum, we measured the equivalent widths of several lines predicted to be strong in the VALD database (Kupka et al., 2000). The abundances were deduced from the equivalent widths using a model atmosphere having $T_{\rm eff} = 10000$ K, $\log g = 3.67$ and [Fe/H] = -1.0 (see Table 1.5).

One caveat regarding these abundances is the use of equivalent widths from single lines with large rotational broadening, since the effect of blending with nearby weak lines cannot be taken into account. A second is that these abundances invariably rely on the strongest lines, which are precisely those most susceptible to departures from local thermodynamic equilibrium. Nevertheless, they do confirm the earlier impression that the star is metal-poor, and justify the adoption of [Fe/H]=-1.0 ± 0.4.

As a second approach to determine the stellar parameters of Tycho-B we used the low resolution spectra observed with LRIS. The observation range of LRIS was chosen to be centered around the Balmer jump as this feature is sensitive to the surface gravity (Bessell, 2007). We fitted the spectra to a grid of model spectra (Munari et al., 2005) using a spectrum fitting tool described below. The final grid we used covered $\log g$ from 3.5 to 4.5 in steps of 0.5 and $T_{\rm eff}$ from 9000 to 12000 K in steps of 500 K. In addition we expanded the grid by reddening the spectra with the *pysynphot*-package[2]. We also added diffuse interstellar bands (Beals & Blanchet, 1937; Herbig, 1966, 1967, 1975, 1995; Hibbins et al., 1994; Jenniskens & Desert, 1994; Wilson, 1958) to the synthetic spectra , which were scaled with reddening . The included E(B-V) ranged from 0.5 to 1.3 in steps of 0.2. We assumed a rotation of 171 km s^{-1} in the grid (see section 1.3.3).

We used χ^2 as a figure of merit in our fitting procedure. To find the best fit for Tycho-B we used the MIGRAD algorithm provided by *MINUIT* (James & Roos, 1975) and linearly interpolated between the grid points using *LinearNDInterpolator* provided by the *scipy*-package Jones et al. (2001). The fit of Tycho-B results in $T_{\rm eff}$=10570 K, $\log g$=4.05, [Fe/H]=-1.1 and E(B-V)=0.85. The model fits the synthetic spectrum poorly in the wavelength region between 3800 – 4280 Å in (see Figure 1.5). The adopted mixing length parameter used in 1D model atmospheres used to construct the spectralgrid influences the fluxes in that region as well as affecting the hydrogen line profiles. Heiter et al. (2002) and others show

[2]pysynphot is a product of the Space Telescope Science Institute, which is operated by AURA for NASA.

that a mixing length of 0.5, rather than 1.25 as used in the Kurucz/Munari grid, better fits the violet fluxes and the hydrogen line profiles. Spectra using a mixing length parameter of 0.5 are brighter in the violet and the H_γ, H_δ and H_β profiles give the same $T_{\rm eff}$as the H_α profiles. We have chosen, however, to fit the spectrum and ignore the problematic spectral region (3800 – 4280 Å) to avoid a systematic error. This yields $T_{\rm eff}$=10722 K, log g=4.13, [Fe/H]=-1.1 and E(B-V)=0.86. The differences are indicative of a systematic error in the model. We adopt the fit excluding the problematic wavelength region in the further analysis. Exploring the complex search space we estimate the error to be $\Delta T_{\rm eff}$=200 K, Δ log g=0.3 and $\Delta[Fe/H]$=0.5, but acknowledge that the parameters are correlated.

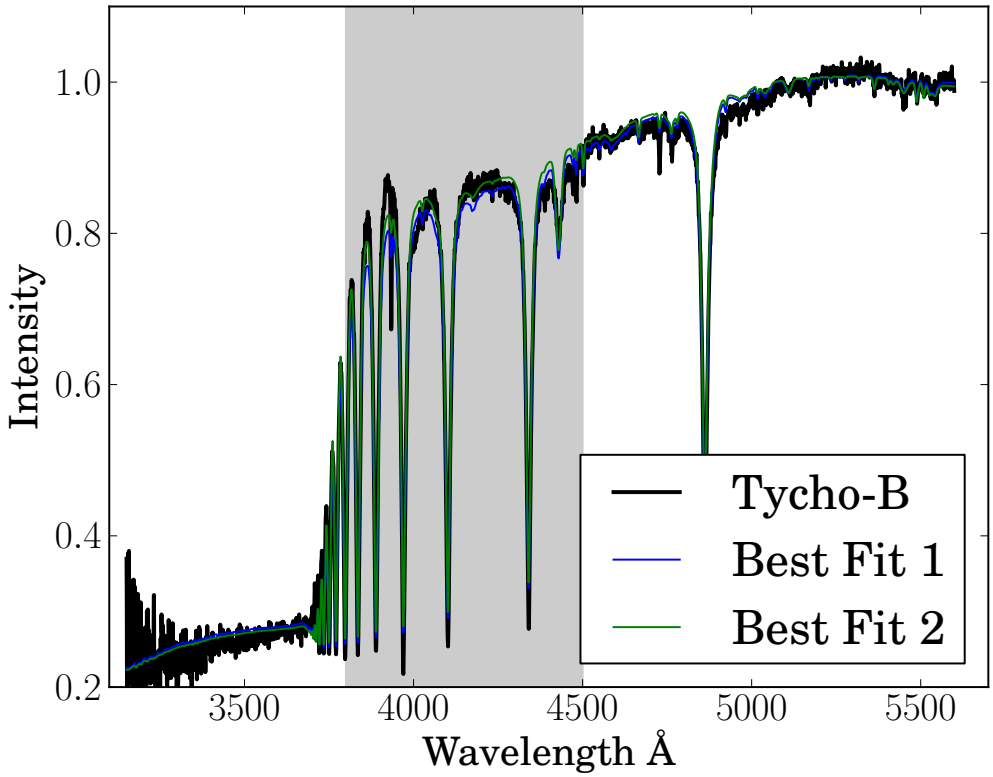

Figure 1.5 The plot shows the normalized spectrum of Tycho-B with the fit which excluded the spectral region between 3800 – 4500 Å(Best Fit 1) and the fit with the problematic region (Best Fit 2). The region is marked with a gray shade.

1.3.5. Distance

To measure the distance to the candidate stars we used colours and absolute magnitude from isochrones by Pietrinferni et al. (2004). We used the MIGRAD algorithm (James & Roos, 1975) to find close matches of the measured values to $T_{\rm eff}$-log g isochrones by varying the age of the isochrone. Subsequently we calculate E(B-V) using the isochrone's colour and we extract a mass from the isochrone. The results can be seen in Table 1.7. To estimate the errors in all distance, reddening and mass we employed the Monte-Carlo method with 10,000 samples of $T_{\rm eff}$, log g, [Fe/H], B- and V-magnitude (see Figure 1.6). Errors included in Table 1.7 are the standard deviations of the Monte-Carlo sample. The data shows that

all stars are compatible with the distance of the remnant. This is not unexpected as the uncertainties of the measurements in stellar parameters are relatively large.

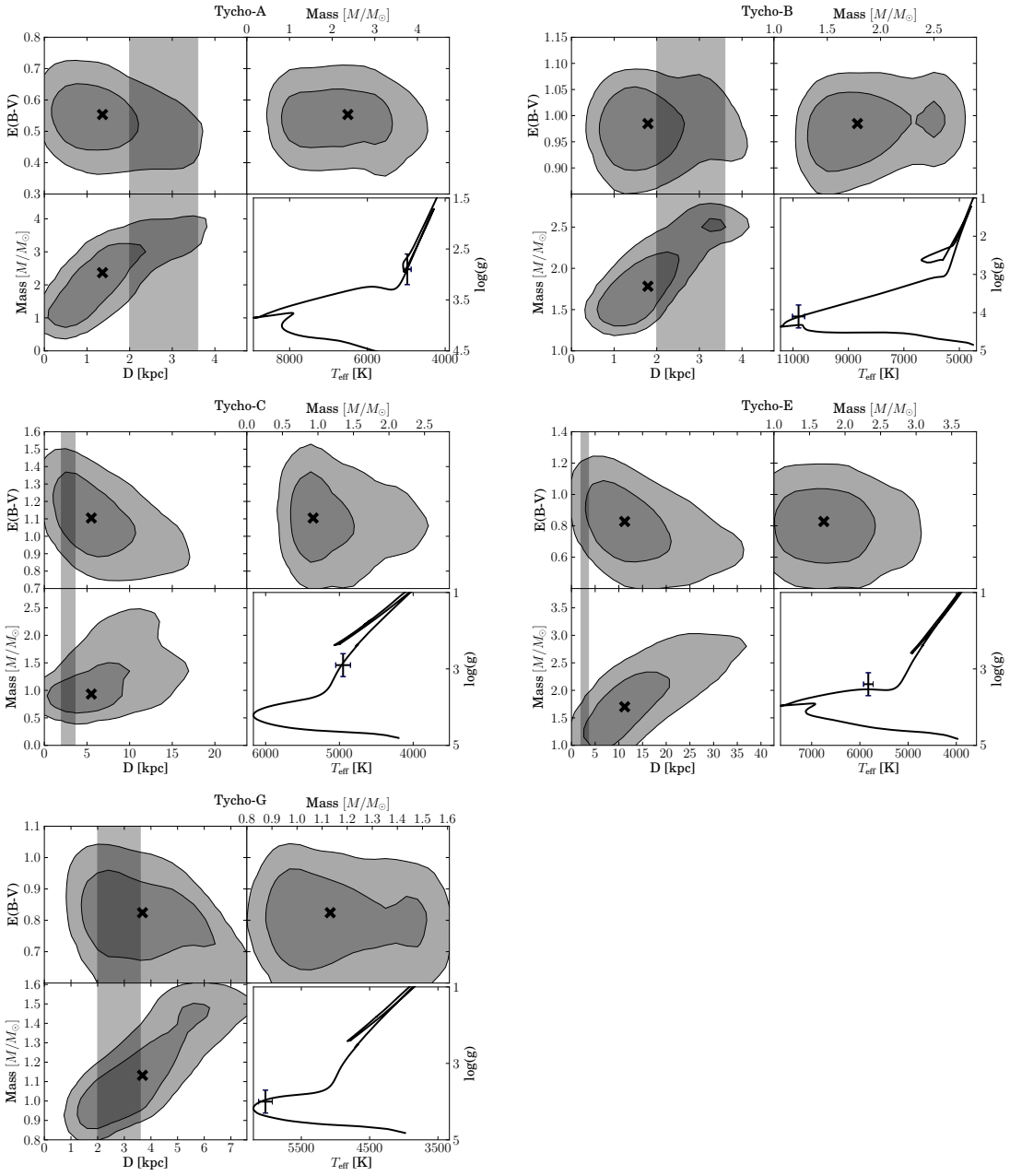

Figure 1.6 The figures show error contours for distance, extinction and mass of the candidates. The lower right shows the optimal isochrone (Pietrinferni et al., 2004) for the measured values of $T_{\rm eff}$ and $\log g$.

Table 1.6 Distances, Ages and Masses of candidate stars

Name designation	Mass $M/M_\odot$	ΔMass $M/M_\odot$	Age Gyr	ΔAge Gyr	Distance kpc	ΔDistance kpc
Tycho-A	2.4	0.8	0.7	2.3	1.4	0.8
Tycho-B	1.8	0.4	0.8	0.3	1.8	0.8
Tycho-C	0.9	0.4	10.0	3.4	5.5	3.5
Tycho-E	1.7	0.4	1.4	1.1	11.2	7.5
Tycho-G	1.1	0.2	5.7	2.1	3.7	1.5

1.4. Discussion

In our sample of six stars we find no star that can be unambiguously identified as a a donor star for SN1572. On the other hand none of the stars in the sample can be completely ruled out.

Tycho-A is a metal rich giant. It seems to be likely that Tycho-A is a foreground star. Its principal redeeming feature as a donor star candidate is that it is located in the geometric center of the remnant, and that it has a relatively low gravity. Tycho-A shows a very low spatial motion which is consistent with a giant donor star scenario. Its lack of rotation, however, is in conflict with said scenario. Taking all measurements into account we regard Tycho-A to be a very weak candidate.

Tycho-B's high temperature, position at the center of the remnant, high rotational velocity and unusual chemical abundance made it a highly unusual candidate in the Tycho Remnant center. Despite the a posteriori unlikely discovery of such a star in the remnant center, Star B's high rotational velocity coupled with its low spatial velocity, seem to be in conflict with viable donor star scenario. These scenarios predict that the donor star will tidally couple to the white dwarf star before explosion, causing the rotation and spatial motion to be correlated post explosion (as discussed in WEK09). The large rotation seen in Tycho-B should accompanied by spatial motion, which is ruled out by the observations presented here, a problem we are unable to reconcile with Tycho-B being the donor star.

Tycho-C consists of two stars which are only resolved in HST images. It consists of a brighter bluer component and a dimmer redder component (difference of one magnitude in all colors) (RP04). In our analysis we find a satisfying solution for the spectrum and suspect that this is from the bluer brighter component. For the brighter bluer component Tycho-C is a metalpoor giant, probably located beyond the remnant. Tycho-C similar to Tycho-A might be compatible with a giant donor star scenario. It's lack of rotation and kinematics, however, make it an uninteresting candidate.

Tycho-D is roughly ten times dimmer than the close star Tycho-C ($\approx 0.6''$). Our tools to measure stellar abundances are not effective for spectra with a S/N less than 10. We however compared the stars by over plotting them and determined that Tycho-D is similar to Tycho-C. Similar to Tycho-C we believe Tycho-D to be a very weak candidate.

Tycho-E is the most distant star in this set (11.2 kpc). It seems to be similar to Tycho-G in temperature, however is a subgiant. It is located 7''from the geometric center and has no unusual stellar parameters or kinematics. Ihara et al. (2007) have looked at iron absorption lines in stellar spectra made by the remnant and found Tycho-E to be unusual. They suggest that a star in the background would show blue and redshifted iron lines, a star inside the

remnant would only show blueshifted iron lines. A foreground star will not show any iron features from the remnant. Ihara et al. (2007) suggest that Tycho-E only shows blue-shifted lines and thus is suggested as being in the remnant. We believe however that Tycho-E is located far behind the remnant and suggest that a low column density on the receding side of the remnant could cause a lack of red-shifted iron features. In summary, a lack of rotation, kinematics and distance make it a very weak candidate.

Tycho-G is located 30'' from the X-Ray center which makes it the most remote object to the center in this work. This work confirms the radial velocity measured by GH09 and WEK09. Figure 1.2 shows the exepected distribution of radial velocities from the Bescançon model of Galactic dynamics. Tycho-G is not a significant outlier at the distance of the remnant as well as behind. In addition, this work has analysed the proper motion of stars around the center of SN1572. Figure 1.1 shows Tycho-G to be a slight outlier, but also shows other stars to be outliers. The kinematic features of a donor star might easily be lost in the kinematic noise of the Galaxy. WEK09, however, suggested using post-explosion stellar rotation as a possible feature for a donor star. This work suggests that Tycho-G has a rotation below the instrumental profile. We find Tycho-G to be a sub-giant star with roughly solar temperature and metallicity. GH09 measure a slight Ni enhancement, which they believe to originate in the contamination from the ejecta. Figure 1.4 compares our measurement of Tycho-G to the distribution of Ni and finds it to be consistent with this distribution. In addition, we could not measure a significantly enhanced Lithium-abundance as suggested in GH09. Finally, we have measured the distance to Tycho-G and believe it to be behind the remnant. Although our error bars make it consistent with the remnant.

In summary, we acknowledge that Tycho-G has unusual kinematics. However, this kinematic predicts rotation for Tycho-G which we do not observe (there are caveats however, see WEK09). We have not found a satisfying explanation for Tycho-G's large distance to the geometric center. We suggest that Tycho-G has the features consistent sub-giant background interloper.

1.5. Conclusion

This work did not detect an unambiguously identifiable donor star candidate. We acknowledge that Tycho-B and Tycho-G have unusual features, but there has been no conclusive explanation for all their parameters. Further theoretical predictions are needed to make a more precise distinction between donors and unrelated stars.

Our observations provide a case that the Tycho SNR does not have a MS, SG, or RG donor star, but other possibilities remain. These include a Helium donor, such as the so-called Sub-Chandra explosions discussed by Livne & Arnett (1995); Sim et al. (2010). These progenitor systems might leave behind a very faint and fast moving He star. Such a progenitor would probably evade detection, and would likely not leave behind traces, such as circum-stellar interaction (henceforth CSI) with the remnant, or early light curve anomalies (Kasen, 2010). However, deep multi-epoch wide field optical images should catch any such star speeding away from the remnant center - these are observation not yet taken. Finally, a double degenerate progenitor, in most cases, does not leave behind a remant , and is consistent with finding no donor star in Tycho SNR.

SN 1006 and Kepler are two other SN Ia remnants in the Milky Way. SN 1006 is far from

the plane and shows no signs of CSI. Kepler SNR, while far from the galaxy plane, shows CSI with its remnant, and has all the indications of what might be expected from a Single Degenerate scenario of MS or lower gravity star (Chiotellis et al., 2011). Observations of these remnant will better establish if there is a continued pattern to the unusual stars in SN Ia remnant centers, or whether the lack of viable donor stars persists in multiple systems.

1.6. Acknowledgments

PYRAF, scipy numpy matplotlib ipython suite, kudritzki, peter wood (for fxcor),Jorge, Onken with HIRES stuff, Amanda with differential rotation

1.7. Line list

Table 1.7 Measured equivalent widths from the Keck HIRES spectra

λ (Å)	χ (eV)	$\log gf$ (dex)	Source	Tycho-A (dex)	Tycho-G (dex)	Tycho-C (dex)	Tycho-E (dex)
5082.35	3.658	-0.59	Reddy03	6.31	6.44		6.2
5088.54	3.85	-1.04	Reddy03	6.19	6.33		
5088.96	3.68	-1.24	Reddy03	6.21			
5094.42	3.83	-1.07	Reddy03	6.1			
5115.4	3.834	-0.28	Reddy03	6.22			
5682.20	4.10	-0.47	RC02	6.34			
5748.351	1.68	-3.26	RC02	6.33		5.74	
5749.297	3.94	-1.99	RC02	6.38			
5847.01	1.676	-3.41	Reddy03	6.26		5.55	
6007.31	1.68	-3.34	RC02	6.2		5.45	
6053.685	4.23	-1.07	RC02	6.33			
6086.28	4.26	-0.52	RC02	6.25	6.22		
6108.116	1.68	-2.44	RC02	6.26	6.11	5.33	
6111.08	4.088	-0.81	Reddy03	6.33		5.38	
6130.14	4.266	-0.94	Reddy03	6.31			
6175.37	4.089	-0.55	Reddy03	6.25	6.35	5.7	
6176.82	4.09	-0.26	Reddy03	6.3	6.27	5.43	6.01
6177.25	1.83	-3.51	Reddy03	6.23			
6186.71	4.10	-0.97	RC02	6.33	6.23		
6204.61	4.09	-1.11	Reddy03	6.32			
6322.17	4.15	-1.17	RC02	6.31			
6370.346	3.54	-1.94	RC02	6.37			
6378.26	4.154	-0.83	Reddy03	6.3		5.81	
6482.80	1.93	-2.63	RC02	6.2		5.38	
6598.60	4.23	-0.98	RC02	6.3		5.74	
6635.12	4.42	-0.83	RC02	6.37			
6643.64	1.68	-2.03	Reddy03	6.48	6.02	5.34	5.97
6767.772	1.83	-2.17	RC02	6.35	6.19	5.67	
6772.32	3.658	-0.97	Reddy03	6.31			
6842.037	3.66	-1.47	RC02	6.4	6.36		
7030.011	3.54	-1.73	RC02	6.42			
7122.197	3.54	0.048	RC02	6.33		5.34	
7261.918	1.95	-2.7	RC02		6.26		
7327.648	3.8	-1.77	RC02	6.38	6.44		
7409.35	3.8	-0.1	RC02			5.24	
7414.502	1.99	-2.57	RC02		6.2	5.57	6.03
7422.275	3.63	-0.129	RC02	6.47		5.32	5.84
7574.048	3.83	-0.58	RC02	6.3	5.97	5.12	
7748.89	3.7	-0.38	Reddy03	6.42	6.17	5.41	6.27
7788.93	1.95	-2.42	RC02			5.87	6.33
7797.59	3.9	-0.35	Reddy03	6.41	6.16	5.59	6.2
7917.44	3.74	-1.5	RC02		6.14		

BIBLIOGRAPHY

Anderson, J. & King, I. R. 2006, PSFs, Photometry, and Astronomy for the ACS/WFC, Tech. rep.

Asplund, M., Grevesse, N., Sauval, A. J., & Scott, P. 2009, ARA&A, 47, 481

Badenes, C., Borkowski, K. J., Hughes, J. P., Hwang, U., & Bravo, E. 2006, ApJ, 645, 1373

Beals, C. S. & Blanchet, G. H. 1937, PASP, 49, 224

Bessell, M. S. 2007, PASP, 119, 605

Bianco, F. B., Howell, D. A., Sullivan, M., Conley, A., Kasen, D., Gonzalez-Gaitan, S., Guy, J., Astier, P., Balland, C., Carlberg, R. G., Fouchez, D., Fourmanoit, N., Hardin, D., Hook, I., Lidman, C., Pain, R., Palanque-Delabrouille, N., Perlmutter, S., Perrett, K. M., Pritchet, C. J., Regnault, N., Rich, J., & Ruhlmann-Kleider, V. 2011, ArXiv e-prints

Castelli, F. & Kurucz, R. L. 2003, in IAU Symposium, Vol. 210, Modelling of Stellar Atmospheres, ed. N. Piskunov, W. W. Weiss, & D. F. Gray, 20P–+

Castelli, F. & Kurucz, R. L. 2004, ArXiv Astrophysics e-prints

Chiotellis, A., Schure, K. M., & Vink, J. 2011, ArXiv e-prints

Foley, R. J. et al. 2003, PASP, 115, 1220

Han, Z. 2008, ApJ, 677, L109

Hayden, B. T., Garnavich, P. M., Kasen, D., Dilday, B., Frieman, J. A., Jha, S. W., Lampeitl, H., Nichol, R. C., Sako, M., Schneider, D. P., Smith, M., Sollerman, J., & Wheeler, J. C. 2010, ApJ, 722, 1691

Heiter, U., Kupka, F., van't Veer-Menneret, C., Barban, C., Weiss, W. W., Goupil, M.-J., Schmidt, W., Katz, D., & Garrido, R. 2002, A&A, 392, 619

Herbig, G. H. 1966, ZAp, 64, 512

Herbig, G. H. 1967, in IAU Symposium, Vol. 31, Radio Astronomy and the Galactic System, ed. H. van Woerden, 85–+

—. 1975, ApJ, 196, 129

—. 1995, ARA&A, 33, 19

Hernandez, J. I. G., Ruiz-Lapuente, P., Filippenko, A. V., Foley, R. J., Gal-Yam, A., & Simon, J. D. 2009, ApJ, 691, 1

Hibbins, R. E., Miles, J. R., Sarre, P. J., & Herbig, G. H. 1994, in The Diffuse Interstellar Bands, ed. A. G. G. M. Tielens, 31–+

Horne, K. 1986, PASP, 98, 609

Hughes, J. P. 2000, ApJ, 545, L53

Ihara, Y., Ozaki, J., Doi, M., Shigeyama, T., Kashikawa, N., Komiyama, K., & Hattori, T. 2007, PASJ, 59, 811

James, F. & Roos, M. 1975, Comput. Phys. Commun., 10, 343

Jeffery, C. S., Woolf, V. M., & Pollacco, D. L. 2001, A&A, 376, 497

Jenniskens, P. & Desert, F. 1994, A&AS, 106, 39

Jones, E., Oliphant, T., Peterson, P., et al. 2001, SciPy: Open source scientific tools for Python [LINK]

Kasen, D. 2010, ApJ, 708, 1025

Kerzendorf, W. E., Schmidt, B. P., Asplund, M., Nomoto, K., Podsiadlowski, P., Frebel, A., Fesen, R. A., & Yong, D. 2009, ApJ, 701, 1665

Kobayashi, C., Umeda, H., Nomoto, K., Tominaga, N., & Ohkubo, T. 2006, ApJ, 653, 1145

Krause, O., Tanaka, M., Usuda, T., Hattori, T., Goto, M., Birkmann, S., & Nomoto, K. 2008, Nature, 456, 617

Kupka, F. G., Ryabchikova, T. A., Piskunov, N. E., Stempels, H. C., & Weiss, W. W. 2000, Baltic Astronomy, 9, 590

Kurucz, R. & Bell, B. 1995, Atomic Line Data (R.L. Kurucz and B. Bell) Kurucz CD-ROM No. 23. Cambridge, Mass.: Smithsonian Astrophysical Observatory, 1995., 23

Leonard, D. C. 2007, ApJ, 670, 1275

Livne, E. & Arnett, D. 1995, ApJ, 452, 62

Matheson, T., Filippenko, A. V., Ho, L. C., Barth, A. J., & Leonard, D. C. 2000, AJ, 120, 1499

Mennekens, N., Vanbeveren, D., De Greve, J. P., & De Donder, E. 2010, A&A, 515, A89+

Munari, U., Sordo, R., Castelli, F., & Zwitter, T. 2005, A&A, 442, 1127

Oke, J. B., Cohen, J. G., Carr, M., et al. 1995, PASP, 107, 375

Pakmor, R., Kromer, M., Röpke, F. K., Sim, S. A., Ruiter, A. J., & Hillebrandt, W. 2010, Nature, 463, 61

Patat, F., Chandra, P., Chevalier, R., Justham, S., Podsiadlowski, P., Wolf, C., Gal-Yam, A., Pasquini, L., Crawford, I. A., Mazzali, P. A., Pauldrach, A. W. A., Nomoto, K., Benetti, S., Cappellaro, E., Elias-Rosa, N., Hillebrandt, W., Leonard, D. C., Pastorello, A., Renzini, A., Sabbadin, F., Simon, J. D., & Turatto, M. 2007, Science, 317, 924

Pietrinferni, A., Cassisi, S., Salaris, M., & Castelli, F. 2004, ApJ, 612, 168

Ramírez, S. V. & Cohen, J. G. 2002, AJ, 123, 3277

Reddy, B. E., Tomkin, J., Lambert, D. L., & Allende Prieto, C. 2003, MNRAS, 340, 304

Reynoso, E. M., Moffett, D. A., Goss, W. M., Dubner, G. M., Dickel, J. R., Reynolds, S. P., & Giacani, E. B. 1997, ApJ, 491, 816

Robin, A. C., Reylé, C., Derrière, S., & Picaud, S. 2003, A&A, 409, 523

Ruiter, A. J., Belczynski, K., & Fryer, C. 2009, ApJ, 699, 2026

Ruiz-Lapuente, P., Comeron, F., Méndez, J., Canal, R., Smartt, S. J., Filippenko, A. V., Kurucz, R. L., Chornock, R., Foley, R. J., Stanishev, V., & Ibata, R. 2004, Nature, 431, 1069

Saio, H. & Nomoto, K. 1985, A&A, 150, L21

Sim, S. A., Röpke, F. K., Hillebrandt, W., Kromer, M., Pakmor, R., Fink, M., Ruiter, A. J., & Seitenzahl, I. R. 2010, ApJ, 714, L52

Sneden, C. 1973, ApJ, 184, 839

Tonry, J. & Davis, M. 1979, AJ, 84, 1511

Tucker, B. E. 2011, Ap&SS, 40

Vogt, S. S., Allen, S. L., Bigelow, B. C., Bresee, L., Brown, B., Cantrall, T., Conrad, A., Couture, M., Delaney, C., Epps, H. W., Hilyard, D., Hilyard, D. F., Horn, E., Jern, N., Kanto, D., Keane, M. J., Kibrick, R. I., Lewis, J. W., Osborne, J., Pardeilhan, G. H., Pfister, T., Ricketts, T., Robinson, L. B., Stover, R. J., Tucker, D., Ward, J., & Wei, M. Z. 1994, in Presented at the Society of Photo-Optical Instrumentation Engineers (SPIE) Conference, Vol. 2198, Society of Photo-Optical Instrumentation Engineers (SPIE) Conference Series, ed. D. L. Crawford & E. R. Craine, 362–+

Warren, J. S., Hughes, J. P., Badenes, C., Ghavamian, P., McKee, C. F., Moffett, D., Plucinsky, P. P., Rakowski, C., Reynoso, E., & Slane, P. 2005, ApJ, 634, 376

Wilson, R. 1958, ApJ, 128, 57

Yong, D., Lambert, D. L., Paulson, D. B., & Carney, B. W. 2008, ApJ, 673, 854

Yu, S. & Jeffery, C. S. 2010, A&A, 521, A85+